

Theoretical aspects of Ostwald ripening in systems with high solubility and high solid volume fraction

Frédéric Gruy, Michel Cournil

► **To cite this version:**

Frédéric Gruy, Michel Cournil. Theoretical aspects of Ostwald ripening in systems with high solubility and high solid volume fraction. *Acta Materialia*, Elsevier, 1996, 44 (6), pp.2537-2545. 10.1016/1359-6454(95)00350-9 . emse-00496967

HAL Id: emse-00496967

<https://hal-emse.ccsd.cnrs.fr/emse-00496967>

Submitted on 29 Jan 2020

HAL is a multi-disciplinary open access archive for the deposit and dissemination of scientific research documents, whether they are published or not. The documents may come from teaching and research institutions in France or abroad, or from public or private research centers.

L'archive ouverte pluridisciplinaire **HAL**, est destinée au dépôt et à la diffusion de documents scientifiques de niveau recherche, publiés ou non, émanant des établissements d'enseignement et de recherche français ou étrangers, des laboratoires publics ou privés.



THEORETICAL ASPECTS OF OSTWALD RIPENING IN SYSTEMS WITH HIGH SOLUBILITY AND HIGH SOLID VOLUME FRACTION

F. GRUY and M. COURNIL

C.P.P.I.-S.P.I.N., Ecole des Mines, 158 Cours Fauriel, 42023 Saint-Etienne, France

Abstract—Many models have been developed to describe Ostwald ripening. The most recent of them have dealt with systems of high solid volume fraction ($\phi > 0.01$). To obtain an exploitable solution, all these models require several simplifications: assumption of low solubility, assumption of motionless fluid phase, no consideration of the spatial arrangement of the grains, analytical or numerical approximation methods. In this paper an unidimensional linear model (row of grains) of Ostwald ripening is proposed which can be applied to the most general and difficult situation, i.e. systems with high volume fraction in highly soluble grains. This model does not require any simplifying assumption. Its validity can be proved from already published theoretical results. Within this model, the spatial arrangement of the grains and the associated connectivity effects which have not been studied so far, can be taken into account. These effects become particularly important at high volume fraction.

Résumé—De nombreux modèles ont été développés pour décrire le mûrissement d'Ostwald. Les plus récents sont relatifs à des systèmes comportant une fraction volumique élevée en solide ($\phi > 0.01$). Pour aboutir à une solution exploitable, tous ces modèles exigent un certain nombre de simplifications: hypothèse de faible solubilité, hypothèse d'immobilité de la phase fluide, non prise en compte de la distribution spatiale des grains, méthodes analytiques ou numériques approchées. Dans cet article est proposé un modèle linéaire (chaîne de grains) du mûrissement d'Ostwald qui peut être appliqué au cas le plus général et le plus difficile possible, c'est-à-dire, celui de systèmes possédant une grande fraction volumique en grains très solubles. Ce modèle n'exige aucune hypothèse simplificatrice. Sa validité est testée à partir de résultats théoriques déjà publiés. Ce modèle permet également de prendre en compte la répartition des grains dans l'espace et les effets de connectivité associés qui n'avaient pu être étudiés jusqu'alors, bien qu'ils deviennent particulièrement importants à grande fraction volumique.

1. INTRODUCTION

Ostwald ripening, or coarsening, of second phase particles is one of the major causes of changes in the particle size distribution (PSD) with time for a given population of grains. It is particularly important for processes such as ageing of precipitates or liquid phase sintering. The first models were proposed by Todes [1], Lifshitz and Slyozov [2] and Wagner [3] (LSW). The model based on the following assumptions:

- infinite sized system;
- very dilute matrix or liquid phase;
- very small volume fraction of grains ϕ ;
- stationary growth/shrinkage of each grain:

$$\frac{dR}{dt} = \frac{C_{eq} \alpha D \Omega}{R} \left(\frac{1}{R_c} - \frac{1}{R} \right), \quad (1)$$

C_{eq} is the equilibrium concentration of solute close to a plane interface of grain; α is the Gibbs–Kelvin radius; Ω is the atomic volume of the solid; R_c is the critical value of the radius, for which the growth rate is equal to 0; t is the time;

- linearization of the Gibbs–Kelvin law.

They predicted an asymptotic behaviour for long spaces of time, characterized by:

- a power relationship of the mean particle size (\bar{R}^3) versus time, when diffusion of the solute in the medium is the rate-determining step:

$$\bar{R}^3 - \bar{R}_0^3 = Kt, \quad (2)$$

where \bar{R}_0 is the initial mean particle size and K is a rate constant;

- a stable PSD.

Many authors performed this work in the framework of the LSW model in order to include the effect of volume fraction, but always for a low volume fraction [4–7]. Their contribution can be summarized by using a modified growth rate for each grain:

$$\frac{dR}{dt} = \frac{C_{eq} \alpha D \Omega}{R} \frac{1}{1 - (R/R_f)} \left[\frac{1}{R_c} - \frac{1}{R} \right] \quad (3)$$

where R_f is the radius of the “influence sphere” of each grain. R_f and R_c are functions of the PSD moments, particularly ϕ .

These authors obtained cubic laws, where the rate constant depends on the volume fraction. The experimental law for the mean radius versus time is also cubic where, after a transient period, a stable PSD is observed. The latter has been assimilated to the theoretical asymptotic PSD, but the experimental PSD is right-skewed, whereas the theoretical one is left-skewed.

These models are based on mean field theories: they only consider interaction between a given grain and an average environment. Hence, the grain population is treated as a whole.

The dynamics of late stage phase separations in two dimensions are dominated by the Lifshitz–Slyozov mechanism. Marqusee [8] studied this phenomenon by including the effects of competition between growing droplets for two-dimensional systems with finite area fractions. His methodology and results are similar to those of precedent authors.

Following the work of Weins and Cahn [9], other theoretical developments have been proposed; they consider the interaction between a given grain and the other grains. This is a more realistic way of describing Ostwald ripening. Moreover, these models can be applied to more concentrated systems [10–12]. Nevertheless, they require a time-consuming numerical resolution for application. Consequently, only partial results on the influence of the volume fraction upon mean radius and PSD versus time are available. More recently, Dehoff’s “communicating neighbour” model [13] took a step forward by relating the growth or shrinkage rate to a characteristic diffusion distance λ :

$$\frac{dR}{dt} = C_{eq} \alpha D \Omega \left\langle \frac{1}{\lambda} \right\rangle \left[\frac{\mu_1}{\mu_2} - \frac{1}{R} \right] \quad (4)$$

where μ_1 and μ_2 are the first and second moments of the size distribution. He obtained a very different result from Lifshitz and Slyozov: when the solid volume fraction drops to zero, dR^3/dt tends to zero according to Dehoff, while it tends to a finite value according to Lifshitz and Slyozov.

All of these authors have studied the asymptotic behaviour of Ostwald ripening. Few researchers have investigated the transient pre-asymptotic evolution.

Fang *et al.* [14] employed a numerical procedure based on the work of Dehoff to simulate the coarsening process statistically. It was found that the PSD changes rapidly in the early stage of coarsening, but considerably more slowly later on. Whatever the initial right-skewed PSD, the distributions evolve towards a common form, which is considerably different from the asymptotic distribution predicted by either the Dehoff or LSW theories.

All the experimentally observed coarsening PSDs are not the expected theoretical asymptotic ones but they, however, may be considered as “stable” [14]. In fact, the rate constant of the cubic law is dependent on the transient moments of the distribution, in particular the instantaneous geometric standard devi-

ation. Brown [15, 16] showed that there are a large number of possible PSDs which correspond to true steady-state conditions at any given volume fraction. An arbitrary initial PSD will develop into a steady-state distribution that is similar to the initial one at large initial radius values.

For the sake of tractability, the previous models, even the most advanced, involve several simplifying assumptions and neglect certain physical aspects. In this paper, we present a new mathematical and numerical tool with several advantages:

- no simplification of the diffusion–reaction problem; in particular, we take into account the possible movements of the grain and of the fluid;
- no averaging of the spatial distribution of the grains; the local grain density is considered here to be an essential parameter, though its influence has been hitherto ignored by other models;
- the possibility of studying the complete evolution of a set of particles with time from the early stages to the possible asymptotic behaviour;
- the possibility of studying the ripening of highly charged systems with high solubility; this situation occurs in particular, in the case of liquid phase sintering [17]. In this work, we only deal with the case of an unidimensional geometry. This situation may appear a little unrealistic, but Mullins and Vinals [18] have developed a linear model of grain growth and proved its usefulness in exposing principal features of the phenomenon. Furthermore, this model has the advantage of enhancing the aspects of connectivity between grains which are ignored by other models.

The aim of this paper is firstly to describe the model and the associated numerical procedure, and secondly to use it to determine the influence of:

- (i) the volume fraction of grains;
- (ii) the initial particle size distribution (PSD) of the grains;
- (iii) the spatial arrangement of the grains.

Lastly, in the discussion section, the conclusions of studies (i) and (ii) will be compared to the results found in the literature. The conclusion of study (iii), which is quite recent, will be qualitatively analyzed. Our main objective is to prove that a rigorous model—although of very simple geometry—is able to confirm the most recent results from the literature and to deal with new situations which the previous models were unable to tackle. A major advantage of our model is the rapidity of the calculations, which enables the exploration of a larger range of physical parameter values.

2. DESCRIPTION OF THE MODEL AND NUMERICAL PROCEDURE

Figure 1 represents the geometry of the unidimensional set of particles. The particles are composed of

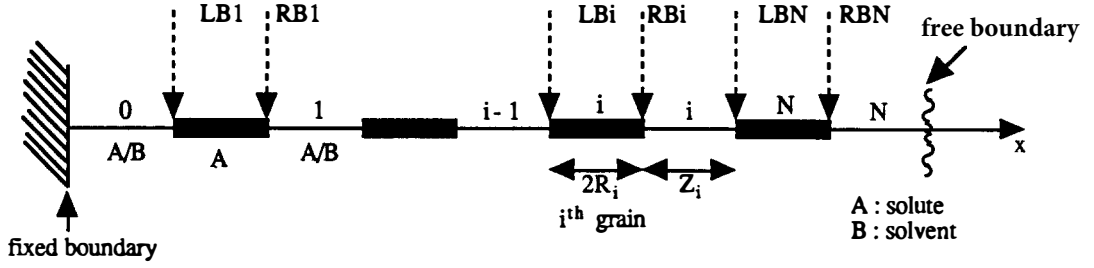


Fig. 1. Geometry of the set of particles.

the solid A (solute), which is soluble in the liquid B (solvent). A grain i is defined by two boundaries, LB_i and RB_i . The left boundary of the whole system is fixed whereas the right boundary may be free to move.

The model can now be built according to the successive steps:

(i) Mass balance equations.

To be representative of dilute as well as concentrated liquid media, the mass balance equations of A must be written in the general form [19, 20]:

$$\frac{\partial \rho_A}{\partial t} = -\frac{\partial}{\partial x} \left(\rho_A v_x - \frac{D}{\rho \bar{V}_B} \frac{\partial}{\partial x} \rho_A \right), \quad (5)$$

where ρ_k , \bar{V}_k are the mass density and mass partial volume, respectively, of component k ; and D is the experimentally measured diffusion coefficient of A into B; v_x is the mean mass velocity along the coordinate x . The total mass balance is expressed by:

$$\frac{\partial \rho}{\partial t} = -\frac{\partial}{\partial x} (\rho v_x) \quad (6)$$

where $\rho = \rho_A + \rho_B$ is the total mass density of the liquid.

(ii) State equation of the liquid phase.

ρ and ρ_A are not independent variables, but are linked by the state equation of the liquid phase which is assumed by Pascal [21] to be expressed as:

$$\rho = \rho_B^0 + a\rho_A \quad (7)$$

where ρ_B^0 is the density of the pure solvent; a is an experimentally measured constant. If mass partial volumes are taken as constant with $\rho_B^0 = \bar{V}_B^{-1}$, the relation (7) can be obtained directly with $a = 1 - \rho_B^0 \bar{V}_A$. It has been observed [19], that the experimental diffusion coefficient in concentrated solution varies little. For the rest of this work it will be taken to be constant.

(iii) Boundary conditions.

The boundary conditions may be found following Vrentas [22]: the conservation of mass at such interfaces can be expressed using the

overall jump mass balance and the jump mass balance for species A and B. The first leads to:

$$\rho(v_x - U) = \rho_s(v_s - U) \quad (8)$$

where U , ρ_s and v_s are, respectively, the velocity of the phase interface, the density of the solid and the mass average velocity in the solid phase.

The second leads to:

$$\text{for A: } \rho_A(v_A - U) = \rho_s(v_s - U) \quad (9)$$

$$\text{for B: } \rho_B(v_B - U) = 0. \quad (10)$$

If it is assumed that the surface kinetics can be described by the following first-order rate expression:

$$\pm \rho_s(U - v_s) = \rho_s k(\rho_A - \rho_{A,eq}) \quad (11)$$

where k is a kinetic constant and $\rho_{A,eq}$ the equilibrium concentration or the solubility of A given by Gibbs–Kelvin law: $\rho_{A,eq} = \rho_{A,eq}^\infty e^{\pm \gamma/R}$. The “+” sign corresponds to the interface RB_i , and the “−” sign corresponds to the interface LB_i .

From equations (5) and (8)–(11), two boundary conditions at any grain–liquid interface can be obtained:

$$\pm \rho_s k(\rho_A - \rho_{A,eq})(\rho - \rho_A) = \frac{D}{\bar{V}_B} \frac{\partial \rho_A}{\partial x} \quad (12)$$

and

$$v_x = U \pm \frac{\rho_s}{\rho} k(\rho_{A,eq} - \rho_A). \quad (13)$$

At the fixed external boundary, these conditions become:

$$\frac{\partial \rho_A}{\partial x} = 0 \quad (14)$$

and

$$v_x = 0. \quad (15)$$

For the moving external boundary:

$$\frac{\partial \rho_A}{\partial x} = 0. \quad (16)$$

(iv) Initial conditions.

At instant zero, the concentration in A is taken to be uniform in the liquid phase:

$$\rho_A = \rho_{A,m}. \quad (17)$$

(v) Time evolution of the grain radii.

From the different boundary conditions, it follows:

$$\frac{d2R_i}{dt} = (U - v_s)_{x=RB_i} - (U - v_s)_{x=LB_i}. \quad (18)$$

The above set of equations [equations (5)–(18)] pose a typical moving boundary problem. Generally speaking, exact solutions of moving boundary problems are available only in a few cases. However, a number of special techniques have been developed to give an approximate solution to the problem. In the present study, we apply the simplest method, i.e. Goodman's integral approximation[23–25]. Its differential steps are:

- the integrated form of the mass balance is written together with boundary conditions in a liquid space;
- the concentration profile ρ_A versus x may be approximated by a quadratic expression in x , the coefficients of which are functions of time and may also be evaluated by applying boundary conditions;
- by introducing the quadratic expression for ρ_A in the integrated form of the mass balance, ordinary differential equations (ODE) for $R_i(t)$ and $Z_i(t) = LB_{i+1} - RB_i$ (liquid domain extension) are obtained:

$$(a-1) \left(\frac{\rho_{A,eq}^i + \rho_{A,eq}^{i+1}}{2} \right) + \frac{1}{2} \frac{\rho_{0B}}{k\rho_s} \frac{dZ_i}{dt} \times \left(1 + \frac{k\rho_s\gamma}{6\rho_{0B}D} Z_i \right) = \delta \frac{Z_i(0)}{Z_i} - \rho_{0B} \quad (19)$$

$$2 \frac{dR_i}{dt} = k \frac{(\rho_{A,eq}^{i-1} - \rho_{A,eq}^i)}{2 + (k\rho_s/D\rho_{0B})\gamma Z_{i-1}} - k \frac{(\rho_{A,eq}^i - \rho_{A,eq}^{i+1})}{2 + (k\rho_s/D\rho_{0B})\gamma Z_i} + \frac{1}{2(a-1)} \frac{\rho_{0B}}{\rho_s} \left(\frac{dZ_{i-1}}{dt} + \frac{dZ_i}{dt} \right) \quad (20)$$

where

$$\gamma = \rho_{0B} + a\rho_{A,eq}^\infty - \rho_{A,eq}^\infty = \rho_{B,eq}^\infty$$

and

$$\delta = \rho_{0B} + a\rho_{A,t=0} - \rho_{A,t=0} = \rho_{B,t=0}.$$

To obtain the equations (19) and (20) in a tractable form, $\rho - \rho_A$ has been replaced by γ in equation (12).

Performing the same sort of transformation as previously, transformed ordinary differential equations can be obtained to represent the time evolution of the external grains and liquid intervals ($i = 1, i = N$) of the system.

We now give the details of the numerical solution to equations (19) and (20). We have considered $N = 1000$ particles. The Euler method has been used to integrate the set of equations. The initial conditions (set of random or predetermined radii) are

indicated below. Given a configuration at time t_s , $\{R_i(t), Z_i(t)\}$ equations (19) and (20) are iterated once for each grain to yield $\{R_i(t + \Delta t), Z_i(t + \Delta t)\}$, where Δt is the step size. A difficulty arises in representing the removal of a grain in both a mathematically and a physically correct manner. We propose the following: as the radius of a given grain decreases, the equilibrium mass concentration $\rho_{A,eq}$ increases according to the Gibbs–Kelvin law; however, the equilibrium concentration is bounded by the density of the solid ρ_s . This value is reached for a certain radius value R_L . When the radius is smaller than R_L , the equilibrium concentration is taken to be equal to ρ_s . A variable step size Δt is used to control the grain removal. Let us assume that a grain has just disappeared (at time t_0) and that i_D represents the next grain which will disappear. The new “initial” concentration in A (in fact, when $t \rightarrow t_0^+$) in any of the liquid intervals is taken to be equal to its respective mean value calculated at the end of the previous step, just before the complete dissolution of the grain, i.e. when $t \rightarrow t_0^-$. Concerning now the grain i_D , at $t = t_0$, it is at a distance of $Z_{i_D-1}(t_0)$ and $Z_{i_D}(t_0)$, respectively, from its left and right neighbour; and the mean density is equal to $\rho_{A_m}^{i_D-1}(t_0)$ on its left side and $\rho_{A_m}^{i_D}(t_0)$ on its right side. After the complete dissolution of grain i_D , which occurs at instant t_1 , it is necessary to calculate the new initial uniform density of A in the interval between the grains $i_D - 1$ and $i_D + 1$ which are now neighbours. For this we propose to use the relation:

$$\rho_{A_m}^{i_D-1}(t_1) = \frac{\rho_{A_m}^{i_D-1}(t_0)Z_{i_D-1}(t_0) + \rho_{A_m}^{i_D}(t_0)Z_{i_D-1}(t_0)}{Z_{i_D-1}(t_1) + Z_{i_D}(t_1)}. \quad (21)$$

This relation is compatible with mass conservation and the integral approximation method. This procedure may be continued until all of the grains have been eliminated. The calculations have been performed on an IBM compatible PC (486/50); each program run takes about 30 min.

Although the numerical procedure involves some simplifications [essentially equations (19) and (20)] we have proved its validity by comparing its results to those given by a finite difference scheme which was applied to the original system of partial derivative equations. The two schemes have been compared for up to 10 grains; they give quite similar results. As the numerical scheme presented here is considerably quicker, it alone has been applied in what follows.

3. RESULTS

In this section, we report results of numerical integration of the ODE system setup above. We examine firstly the variation in the mean radius and the PSD; we also emphasize the influence of the initial volume fraction and PSD, with the aim of comparing our results with other model results. Then, we study the influence of the grains' relative location, an

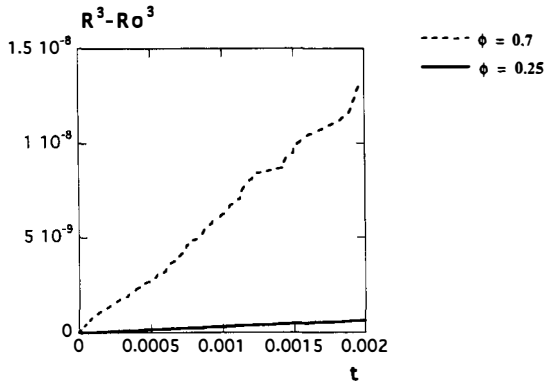


Fig. 2 $\bar{R}^3 - R_0^3$ versus time for different fractions. R and t are normalized by L_0 and $L_0^2 D^{-1}$, respectively.

investigation which can be performed using our model.

The application field of our model is too large to examine all the possible cases. A set of typical parameter values commonly met in other theoretical works has been chosen:

$$\frac{\rho_{A,eq}^\infty}{\rho_{0B}} = 0.3; \quad \frac{\rho_{0B}}{\rho_s} = 0.2;$$

$$\frac{\rho_{A,in}(t=0)}{\rho_{0B}} = 0.3; \quad a = 0.2; \quad \frac{\alpha}{L_0} = 10^{-5}.$$

L_0 is the overall initial system size. The ratio $L_0 \rho_s k / D$ has been so defined that it can be varied if so desired, because this parameter compares the diffusion to the interfacial reaction rate.

- (i) Influence of the volume fraction. For the first simulations, the initial condition is a set of randomly chosen radii uniformly distributed between 0 and $2\bar{R}$. The grains are randomly placed. The initial intergranular distances, either $Z_i(0)$ or $R_i(0) + Z_i(0) + R_{i+1}(0)$ are taken to be constant. The results are the same for the two cases. When the interface reaction is the rate-limiting step, a parabolic law is observed

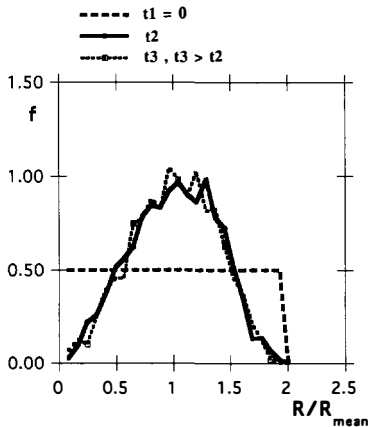


Fig. 3. Evolution of the reduced particle size distribution ($\phi = 0.25$).

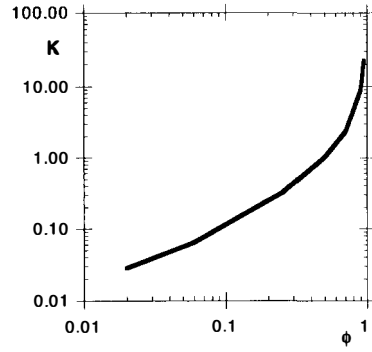


Fig. 4. Kinetic constant of the cubic law versus volume fraction.

for the variation of the mean radius with time. When the solute diffusion is the rate-limiting step, a cubic law is observed (Fig. 2). This is true whatever the volume fraction. This result agrees with LSW and related theories. From now on, we will deal with evolutions where the diffusion is the rate-limiting step. We have verified that a cubic law is observed to be in agreement with these theories, not only during the period of asymptotic behaviour, but also as early as the first stage of the process. This behaviour was recently mentioned by Patterson and co-workers [14, 26]. The reduced PSD has been calculated for different steps of Ostwald ripening ($\phi = 0.25$; Fig. 3). It tends to a quasi-stable form which is independent of the rate-limiting step. The standard deviation tends to a certain limit ($\sigma_{qs} = 0.35$). The skewness is negative but small ($S_{qs} = -0.25$). This indicates that the PSD shape is nearly symmetrical. Figure 4 represents the kinetic constant of the cubic law K versus the volume fraction ϕ for ϕ values between 0.02 and 0.95. Below the value of 0.02, the mean radius versus time does not obey a cubic law. Both the standard deviation and the skewness approach stable values after relatively rapid changes in the early stages of coarsening. These stable values

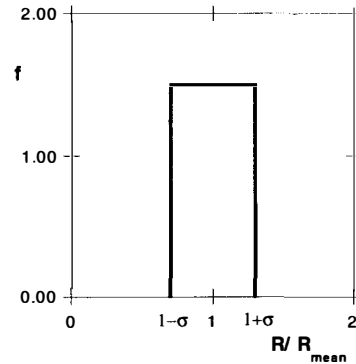


Fig. 5. Rectangular initial particle size distribution.

Table 1. Kinetic constant K , standard deviation σ and skewness S as a function of the initial PSD width (initial centre-centre intergranular distances are taken as constant)

σ	0.1	0.25	0.5	0.75	1
$K (\times 10^6)$	0.25	0.245	0.28	0.33	0.38
σ_{qs}	0.3	0.3			0.35
S_{qs}	-0.35	-0.4			-0.25

are not highly dependent upon the volume fraction ($\sigma_{qs} = 0.34 \pm 0.02$; $S_{qs} = -0.25 \pm 0.05$).

- (ii) Influence of the initial particle size distribution. We have studied the effect of initial PSD shape on the kinetic constant and the PSD parameters for the same volume fraction $\phi = 0.25$. For an initial PSD which is rectangular in shape (characterized by its half-width σ , Fig. 5), we have found that, as σ increases, the kinetic constant also increases and the quasi-stable PSD becomes slightly wider and more symmetrical (Table 1). For an initial log-normal PSD (characterized by the geometric standard deviation $\ln \sigma$), we found that as $\ln \sigma$ increases, the kinetic constant increases and the quasi-stable PSD is slightly wider and more symmetrical. For $\ln \sigma = 0.5, 0.67$ and 1 , the decrease of σ and S from their initial values is slow. It is not certain that the quasi-stable state is reached (Table 2). One can conclude that, as the initial PSD widens, the kinetic constant of the cubic law increases and the quasi-stable PSD becomes a little wider and more symmetrical. The shape of the curve of $\bar{R}^3(t)$ in the early stages of coarsening, i.e. before the quasi-stable state, depends on the initial PSD: for a random narrow distribution the curve is concave, and for a random wide distribution the curve is convex. This is in agreement with the results of Patterson [14].
- (iii) Influence of arrangement of the grains. It is obvious that the relative position of the different grains is an important factor in the early stages of coarsening. In order to investigate it, we have tested three arrangements of particles, using a volume fraction of $\phi = 0.25$ and an initially rectangular ($\sigma = 1$) PSD. In Figs 6-11, the arrangement and the function $\bar{R}^3 - R_0^3 = f(t)$ are shown. Only in the case of an initially random arrangement does $\bar{R}(t)$ obey a cubic law [Figs 8 and 11]. In the case

Table 2. Kinetic constant K , standard deviation σ and skewness S as a function of the initial PSD width (initial boundary-boundary intergranular distances are taken as constant)

$\ln \sigma$	0.05	0.2	0.5	0.67	1
$K (\times 10^6)$	0.26	0.285	0.35	0.42	
σ_{qs}	0.3	0.32	0.32	0.33	0.37
S_{qs}	-0.5	-0.4	-0.25	-0.11	0

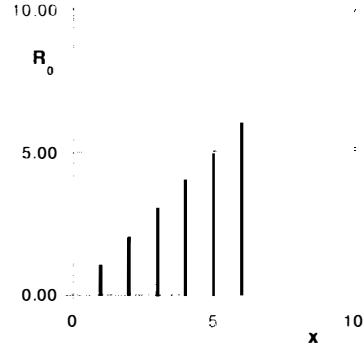


Fig. 6. Initial particles arrangement defined by $R_0[i] = i/N$; $1 < i < N$.

corresponding to Fig. 6, the initial regular arrangement is very smooth; therefore the changes in the particle set are slow and the quasi-stable state is not reached (Fig. 9). In the case corresponding to Fig. 7, the initial arrangement is the most irregular possible. It can be seen [Fig. 10] that after a strong increase, $\bar{R}^3 - \bar{R}_0^3$ rises very slowly. This corresponds approximately to the rapid removal of half the initial number of particles followed by the evolution of a more regular arrangement.

4. DISCUSSION AND CONCLUSION

The validity of our discrete and unidimensional model will be firstly examined via a comparison with the most advanced of the previously proposed theories.

- Asymptotic (or quasi-stable) behaviour. After a transient period, $\bar{R}(t)$ verifies a parabolic law when the interface reaction is rate-limiting and a cubic law in the case of slow diffusion. These results are in agreement with the prediction of all previous theories. The particle set rapidly approaches a quasi-stable state, characterized by a reduced PSD, which does not depend on the volume fraction. It is different from the asymptotic PSD deduced from continuous

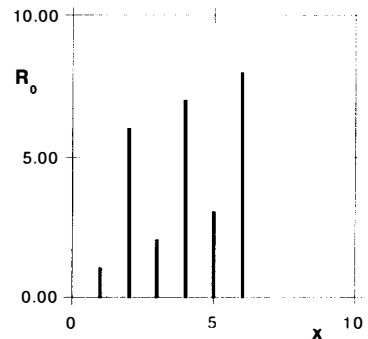


Fig. 7. Initial particles arrangement defined by $R_0[2i+1] = i+1$; $R_0[2i+2] = (N/2) + i+1$; $0 \leq i \leq (N/2) - 1$.

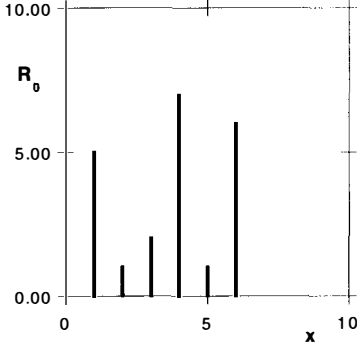


Fig. 8. Initial random particles arrangement.

theory. The simulated PSD is wider and less left-skewed than the asymptotic ones.

- Influence of the volume fraction. From Fig. 4, we can calculate that the dimensionless kinetic constant K and ϕ are related by:

$$K \approx 10^{-6} \frac{\phi}{1-\phi}. \quad (22)$$

This relation can be partially interpreted by the communicating neighbours theory from Dehoff [13]: in this framework, the growth law is given by equation (4). For unidimensional geometry, the diffusion length scale λ is such that:

$$\left\langle \frac{1}{2\lambda} \right\rangle = \frac{N}{L(1-\phi)} = \frac{\phi}{(1-\phi)2\bar{R}} \quad (23)$$

where N is the grains number and L is the system dimension. The mean space between two grains is equal to twice the diffusion length scale. This can be understood by writing:

$$\begin{aligned} \frac{dR}{dt} &\approx \frac{D \Delta \rho}{\rho_s Z} = \frac{D \rho_{i+1} - \rho_i}{\rho_s Z} \\ &= \frac{D}{\rho_s Z} \left(\rho_{i+1} - \frac{(\rho_i + \rho_{i+1})}{2} \right) 2 \\ &= \frac{D (\rho_{i+1} - \bar{\rho})}{\rho_s Z/2}. \end{aligned} \quad (24)$$

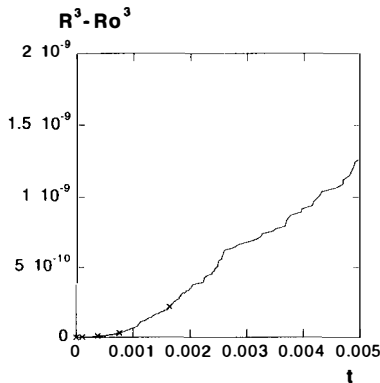


Fig. 9. $\bar{R}^3 - \bar{R}_0^3$ versus time (dimensionless variables) (particles arrangement defined in Fig. 6).

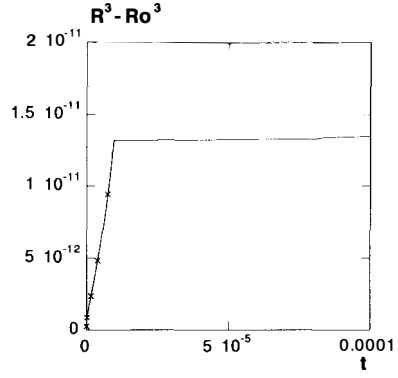


Fig. 10. $\bar{R}^3 - \bar{R}_0^3$ versus time (dimensionless variables) (particles arrangement defined in Fig. 7).

Then the growth law is:

$$\frac{dR}{dt} = \rho_{eq}^{\infty} \frac{\alpha D}{\rho_s} \frac{\phi}{(1-\phi)\bar{R}} \left[\frac{1}{R_c} - \frac{1}{R} \right] \quad (25)$$

where R_c is the already defined critical radius. Classical theories predict that, after a relatively long time, coarsening microstructures achieve a condition in which all of the relative length scales are maintained while the absolute length scale increases [27]. This scale factor growth condition is characterized by an invariant normalized PSD function: if the particle size is expressed in terms of the normalized quantity $r = R/R_c$, it is invariant with time. This distribution function may be derived for any assumed form of particle growth rate equation by integration of the continuity equation relating the number of particles to particle size and time [2, 13]. By using equation (25) the normalized asymptotic distribution function is:

$$g(r) = 5.43 \frac{r}{(2-r)^3} e^{-2/(2-r)}. \quad (26)$$

The standard deviation and the skewness are, respectively, equal to 0.344 and -0.71 . We also obtain the cubic law:

$$\bar{R}^3 - \bar{R}_0^3 = 1.07 \rho_{eq}^{\infty} \frac{\alpha D}{\rho_s} \frac{\phi}{1-\phi} t. \quad (27)$$

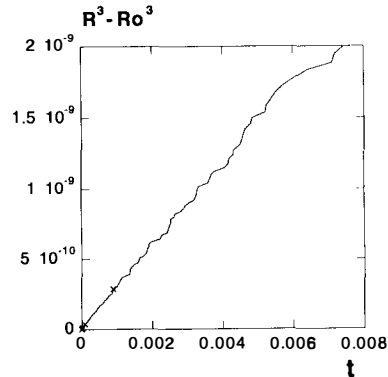


Fig. 11. $\bar{R}^3 - \bar{R}_0^3$ versus time (dimensionless variables) (random particles arrangement of Fig. 8).

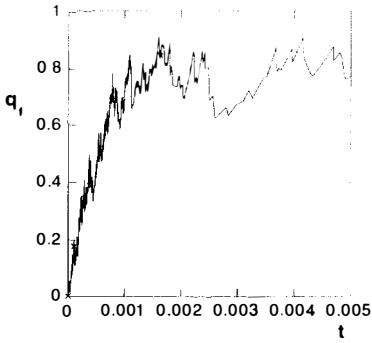


Fig. 12. Smoothing parameter versus time (dimensionless variables) (particles arrangement defined in Fig. 6).

Using the values for the parameters given above, the dimensionless kinetic constant is equal to:

$$K = 0.64 \times 10^{-6} \frac{\phi}{1-\phi}. \quad (28)$$

It should be noted that the classical theory disregards the concentrated solution in the liquid phase. To compare both kinetic constants, we have to multiply the classical kinetic constant by ρ_{0B}/γ [see equation (20)]. Then, using the values of the parameters already given above, the calculated kinetic constant is equal to:

$$K = 0.84 \times 10^{-6} \frac{\phi}{1-\phi}. \quad (29)$$

We obtain good agreement with Dehoff's theory for the function $\bar{R}(t)$, although the asymptotic distribution function is different from the quasi-stable distribution function calculated from our simulation. We cannot explain this discrepancy. Fang and Patterson also observed that the simulated distributions are wider and less left-skewed than the theoretical ones [14].

- Influence of the initial PSD. The kinetic constant of the cubic law (and to a lesser extent the width and symmetry of the quasi-stable PSD) increases with the initial PSD width. These results are in good agreement with those of Fang, Patterson and Turner. This may seem erroneous for the PSD, but in both works the quasi-stable PSD

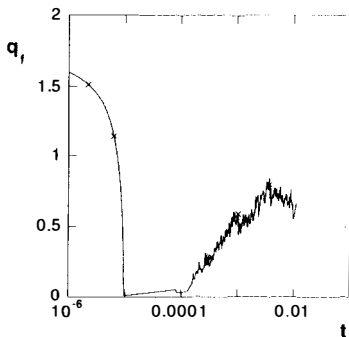


Fig. 13. Smoothing parameter versus time (dimensionless variables) (particles arrangement defined in Fig. 7).

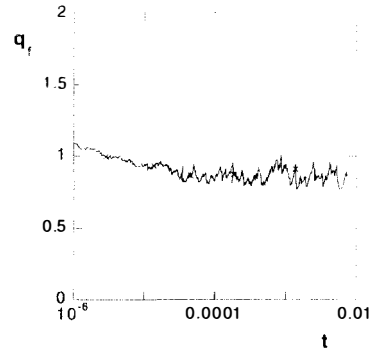


Fig. 14. Smoothing parameter versus time (dimensionless variables) (particles arrangement defined in Fig. 8).

shape does not change greatly with the initial PSD width (Fig. 3, [14]) and the distribution parameters have a similar variation with time (Fig. 4, [14]). Our results, however, seem to be contradictory to those of Brown [15, 16]: we have not observed that any arbitrary initial PSD will develop towards a steady-state distribution that is similar to the initial one at large radius values.

- Influence of the initial particle arrangement. From the experiments reported in Figs. 6–11, it can be concluded that in the early stage of coarsening, the relevant parameter is a smoothing function of the particles set. The simplest way to define the smoothing function q_t is:

$$q_t^2 = \frac{1}{N} \sum_{i=1}^N \left(\frac{2R_i - R_{i-1} - R_{i+1}}{\bar{R}} \right)^2. \quad (30)$$

Figures 12–14 represent q_t versus time for the three initial arrangements. Figures 15–17 represent $\bar{R}^3 - \bar{R}_0^3$ versus z defined by $dz = q_t dt$. We observe large variations of the smoothing function, but nevertheless q_t tends to the same limit $q_t^1 = 0.80$. This value is independent of the volume fraction. At first order, we may approximate equation (30) and write:

$$q_t^2 \approx \frac{1}{N} \sum_{i=1}^N \left(\frac{2R_i - 2\bar{R}}{\bar{R}} \right)^2 = 4\sigma^2. \quad (31)$$

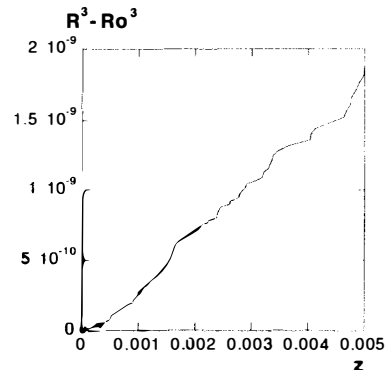


Fig. 15. $\bar{R}^3 - \bar{R}_0^3$ versus $z = \int_0^t q_t dt$ (dimensionless variables) (particles arrangement defined in Fig. 6).

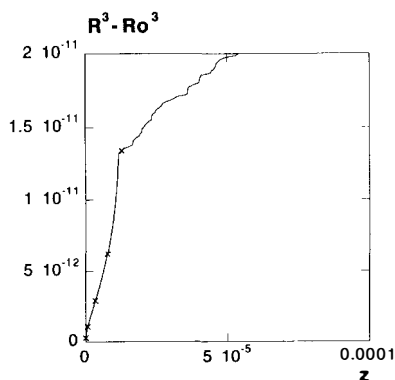


Fig. 16. $R^3 - \bar{R}_0^3$ versus $z = \int_0^t q_f dt$ (dimensionless variables) (particles arrangement defined in Fig. 7).

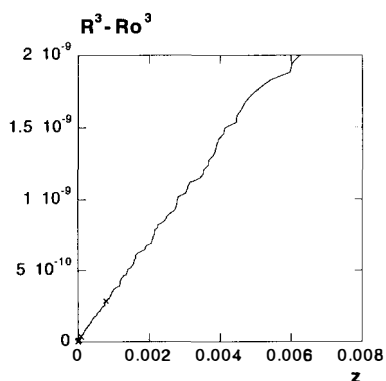


Fig. 17. $R^3 - \bar{R}_0^3$ versus $z = \int_0^t q_f dt$ (dimensionless variables) (particles arrangement defined in Fig. 8).

Hence: $q_f^1 = 2\sigma_{qs}$. Taking σ_{qs} as being nearly equal to 0.35, from the results reported in Table 1, q_f^1 is found to equal 0.7. By using the asymptotic distribution function $g(r)$ from DeHoff theory, we would obtain a lower value: $q_f^1 = 0.59$. Figures 15–17 show that the growth rate $d\bar{R}^3/dt$ is a function of q_f . This is not surprising when we examine equation (20) when $k\rho_s L_0/D$ is infinite (diffusion rate-determining step) and α is small (linearized Gibbs–Kelvin). So we have proved the importance of the initial particle arrangement during the early stage of coarsening. The relevant parameter for this effect characterizes the instantaneous smoothing; it is similar to the instantaneous distribution width used by Fang *et al.* [14] to study the early stages of random arrangement coarsening.

We have set up a mathematical and numerical tool which can be used to study different situations of Ostwald ripening. This model, although only unidimensional, reproduces the most recent results known in this area. Moreover, it has the originality to be adapted to studies of the influence of spatial grain arrangement. As the calculations are simple and rapid, the application of this method means that a large number of numerical test can be performed.

REFERENCES

1. O. M. Todes, *J. Phys. Chem. (Sov.)* **20**, 629 (1946).
2. I. M. Lifshitz and V. V. Slyozov, *J. Phys. Chem. Solids* **19**, 35 (1961).
3. C. Wagner, *Z. Elektrochem.* **65**, 581 (1961).
4. R. Asimow, *Acta metall.* **11**, 72 (1963).
5. A. J. Ardell, *Acta metall.* **20**, 61 (1972).
6. A. D. Brailsford and P. Wynblatt, *Acta metall.* **27**, 489 (1979).
7. K. Tsumuraya and Y. Miyata, *Acta metall.* **31**, 437 (1983).
8. J. A. Marqusee, *J. Chem. Phys.* **81**, 976 (1984).
9. J. J. Weins and J. W. Cahn, *Sintering and Related Phenomena*, p. 151. Plenum Press, New York (1973).
10. P. W. Voorhees and M. E. Glicksman, *Acta metall.* **32**, 2001 (1984).
11. P. W. Voorhees and M. E. Glicksman, *Acta metall.* **32**, 2013 (1984).
12. P. W. Voorhees and M. E. Glicksman, *Metall. Trans. A* **15A**, 1081 (1984).
13. R. T. Dehoff, *Acta metall. mater.* **39**, 2349 (1991).
14. Z. Fang, B. R. Patterson and M. E. Turner, *Acta metall. mater.* **40**, 713 (1992).
15. L. C. Brown, *Acta metall. mater.* **37**, 71 (1989).
16. L. C. Brown, *Acta metall. mater.* **40**, 1293 (1992).
17. S. C. Yang and R. M. German, *J. Am. Ceram. Soc.* **74**, 3085 (1991).
18. W. W. Mullins and J. Vinals, *Acta metall. mater.* **41**, 1359 (1993).
19. J. Newman and T. W. Chapman, *AIChE J.* **19**, 343 (1973).
20. R. A. Robinson and R. H. Stokes, *Electrolyte Solutions*. Butterworths, London (1968).
21. P. Pascal, *Nouveau traité de chimie minérale*. Masson, Paris (1966).
22. J. S. Vrentas and C. M. Vrentas, *Chem. Engng Sci.* **44**, 3001 (1989).
23. S. G. Chatterjee and C. Tien, *Chem. Engng Sci.* **44**, 2283 (1989).
24. B. Sudhakar, *Chem. Engng Sci.* **47**, 475 (1992).
25. F. Gruy and M. Cournil, *Proc. 4ème Congrès Génie des Procédés*, (Edited by Lavoisier), Grenoble (1993).
26. Z. Fang and B. R. Patterson, *Acta metall. mater.* **41**, 2017 (1993).
27. F. Gruy, *Ann. Chim. Fr.* **18**, 69 (1993).